AIAA JOURNAL
Vol. 49, No. 8, August 2011

Effects of Flapping Wing Kinematics on Hovering and Forward Flight Aerodynamics

Hiroto Nagai* and Koji Isogai†
Nippon Bunri University, Oita 870-0397, Japan

DOI: 10.2514/1.J050968

The effects of wing kinematics on the aerodynamic characteristics of a flapping insect wing are investigated experimentally. The time-varying aerodynamic forces acting on the flapping wing are measured in hovering and forward flight using a dynamically scaled mechanical model in a water tunnel, which simulates a bumblebee flapping wing in hovering and forward flight. Wing kinematics can be categorized as trapezoidal or sinusoidal types. The trapezoidal flapping motion is divided into translational and reversal phases, and the trapezoidal feathering motion is divided into fixed-angle and rotational phases. In the sinusoidal type, the time histories of angles for the flapping and feathering motions are represented as sinusoidal functions. The feathering rotation during the flapping translation causes an increase in aerodynamic power rather than lift and thrust for hovering and forward flight. Therefore, it is preferable for the feathering rotation to be conducted during the flapping reversal phase for high efficiency. The trapezoidal flapping motion and trapezoidal feathering motion with a shorter duration of rotation should be selected for a higher efficiency in hovering and forward flight. This result indicates that many insects using the trapezoidal type attach importance to a good efficiency in selecting the wing kinematics. For a larger lift in hovering and slower forward flight, the sinusoidal flapping motion and trapezoidal feathering motion with a shorter duration of rotation should be selected.

Nomenclature

C_N, C_L, C_T	=	normal fluid force, lift, and thrust coefficients
C_P	=	power coefficient
f	=	flapping frequency
F_n	=	normal force
J	=	advance ratio, U_0/V_0
L	=	lift
P	=	power
T	=	thrust
t^*	=	nondimensional time, ft
U_0	=	forward velocity
V_{in}	=	relative inflow velocity
V_0	=	reference velocity
η	=	propulsive efficiency
θ, θ_0	=	feathering angle and amplitude of feathering angle
τ_a	=	duration of rotational acceleration
τ_f	=	timing of rotation
τ_r	=	duration of rotation
τ_t	=	duration of stroke reversal
ϕ, ϕ_0	=	flapping angle and amplitude of flapping angle
ψ	=	stroke plane angle

Superscript

-	=	time-averaged (during one cycle) value

Presented at the 26th Congress of International Council of the Aeronautical Sciences, Anchorage, AK, 14–19 September 2008; received 30 September 2010; revision received 15 March 2011; accepted for publication 16 March 2011.

*Assistant Professor, Department of Aeronautics and Astronautics; nagai@nbu.ac.jp. Senior Member AIAA.

†Visiting Professor, Department of Aeronautics and Astronautics; isogai@nbu.ac.jp. Associate Fellow AIAA.

I. Introduction

INSECTS have unique flying capabilities: i.e., the ability to hover and turn abruptly in addition to the usual cruising flight. The amazing flying capabilities of insects are achieved through the control of wing kinematics. The wing kinematics of insects mainly consist of flapping and feathering motions. The flapping motion is a rotation of the wing around the body axis (upstoke and downstroke), and the feathering motion is a rotation around the span axis of the wing (pronation and supination). Azuma and Watanabe observed the wing kinematics of dragonflies in free flight [1]. Dudley and Ellington measured the wing kinematics of bumblebees [2,3]. Ellington measured those of various insects, such as flies and bees [4]. The time histories of the wing kinematics of insects are represented as very complicated waveforms.

Since insects have very small sizes and high flapping frequencies, unsteady force and flow produced by their flapping wings are difficult to measure directly; hence, experimental simulations using a dynamically scaled mechanical model and numerical simulations using computational fluid dynamics (CFD) have proved to be powerful tools in investigating the aerodynamic mechanisms of insect flapping wings. In experimental and numerical simulations, the time histories of wing kinematics have been represented as simple functions. Sane and Dickinson [5,6], Dickinson et al. [7], Birch and Dickinson [8], Lehmann et al. [9], Birch et al. [10], and Dickson and Dickinson [11] have divided the wing kinematics into flapping translational phases and feathering rotational phases; they also clarified the unsteady aerodynamic mechanisms occurring in flapping wings, such as delayed stall, rotational circulation, and wake capture. Their wing kinematics have been classified as a trapezoidal type and have been employed in many studies [12–17]. Isogai et al. [18] and Yamamoto and Isogai [19] represented wing kinematics as a sinusoidal function and conducted experimental and numerical simulations. Liu et al. [20], Aono and Liu [21], and Aono et al. [22] represented wing kinematics as a Fourier series and simulated insect wing kinematics with CFD. Nagai et al. have conducted experimental and numerical simulations in hovering and forward flight for an insect flapping wing and investigated the unsteady aerodynamics occurring in flapping forward flight with a trapezoidal type of wing kinematics [23].

Although the time histories of insect wing kinematics are very complicated, engineers expect simple, efficient wing kinematics for flapping-type micro air vehicles (MAVs). Kaya and Tuncer

optimized a nonsinusoidal wing path for a two-dimensional (2-D) flapping wing using a NACA0012 airfoil at $Re = 10,000$ to obtain maximum thrust and/or propulsive efficiency in forward flight [24]. Using an elliptic airfoil, Tang et al. numerically simulated a 2-D flapping wing at $Re = 75$–1700 and compared the wing kinematics in normal hovering mode and water-treading mode [25]. Bos et al. numerically simulated a 2-D flapping wing in hovering flight at $Re = 110$ and compared the aerodynamic performances among the four different wing kinematics: sinusoidal, trapezoidal, and two more-realistic fruit fly types [26]. However, these findings did not provide sufficient insight into the wing kinematics required of flapping-type MAVs. Most flapping-type MAVs have three-dimensional (3-D) flapping wings and need to generate both lift and thrust to achieve hovering and forward flight. The time-varying aerodynamic forces are different between the 2-D and 3-D flapping wings because of the difference in the stability of the leading-edge vortex attached on the wing upper surface [27].

In this study, we experimentally investigate the effects of 3-D flapping wing kinematics on the aerodynamic characteristics in hovering and forward flight. Unsteady aerodynamic forces and power are measured using a dynamically scaled mechanical model placed in a water tunnel, which simulates an insect flapping wing in hovering and forward flight. Wing kinematics are categorized as trapezoidal and sinusoidal. Trapezoidal flapping motion is divided into translational and reversal phases, and the trapezoidal feathering motion is divided into fixed-angle and rotational phases. In the sinusoidal type, the time histories of angles for the flapping and feathering motions are represented as sinusoidal functions. Time-averaged aerodynamic characteristics are compared among the following three combinations of motion types: trapezoidal flapping with trapezoidal feathering, sinusoidal flapping with trapezoidal feathering, and sinusoidal flapping with sinusoidal feathering. In addition, we relate the wing kinematics to the time-varying force generation and explain the wing kinematics for high aerodynamic performance.

Considering the feasibility of the hand-sized flapping-type MAV, we select a bumblebee, *Bombus terrestris*, as a model in this study, which has a larger size and better flight capabilities, such as hovering and quick turning, than other insects. The planform, flapping and feathering amplitudes, and stroke plane angle were fixed, but the wing kinematics were changed. Since it is still unclear how the wing planform influences the aerodynamic force and flowfield, we selected the planform of the bumblebee that probably had better aerodynamic performance.

The outline of this paper is as follows. In Sec. II, the experimental method is described. The aerodynamic characteristics among the different wing kinematics are compared in hovering flight in Sec. III, and we discuss the combinations between a flapping phase and a feathering phase. The aerodynamic characteristics in forward flight are discussed in Sec. IV, and concluding remarks are given in Sec. V. In the Appendix, the experimental results are compared with the numerical simulation.

II. Experimental Methods

A. Motion Kinematics of a Flapping Wing

Three orthogonal coordinate systems were employed for a flapping wing, as shown in Fig. 1. The origin O is at the base of the starboard wing, the Z axis is along the vertically downward direction, and the X axis is along the direction of forward flight; $OXYZ$ forms a right-handed Cartesian coordinate system. The z axis coincides with the flapping axis; therefore, the x-y plane coincides with the stroke plane. The stroke plane is horizontal in hovering flight; however, it is tilted at an angle ψ around the Y axis in forward flight. The coordinate system $o_w x_w y_w z_w$ is fixed with the starboard wing and rotates with the wing. The y_w axis coincides with the feathering axis of the wing, and the z_w axis is parallel to the wing chord direction. The flapping angle ϕ is defined as the angle between the y_w and y axes, and the feathering angle θ is defined as the angle between the z_w and z axes. The aerodynamic force acting on the wing is divided into a normal force F_n and a tangential force F_t. It is also divided into a vertical component L (lift) and a horizontal component T (thrust).

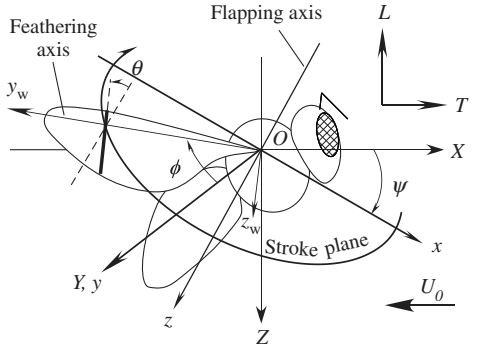

Fig. 1 3-D coordinate systems of a flapping wing.

We employed two simple types of wing kinematics: trapezoidal and sinusoidal. In the trapezoidal type, the time histories of angular velocity for the flapping and feathering motions are represented as trapezoidal functions. In the sinusoidal type, those are represented as sinusoidal functions. Figures 2a and 2b show the time histories of the trapezoidal flapping and feathering motions, respectively. The trapezoidal flapping motion can be divided into two phases: translational and reversal. In the translational phase, the wing moves at a constant flapping velocity. In the reversal phase, the wing decelerates and accelerates at a constant rate around the flapping reversal points. The duration of the reversal phase is denoted by a reversal time τ_t, which is nondimensionalized by the flapping period. The trapezoidal feathering motion can also be divided into two phases: fixed-angle and rotational. The wing moves at a constant angle of attack in the fixed-angle phase; then, the wing rotates around the feathering axis in the rotational phase. The time duration of the rotational phase is denoted by a nondimensional time τ_r, and the duration of rotational acceleration for the feathering motion is denoted by τ_a. In this study, the parameters of the trapezoidal type were determined as follows: $\tau_t = 0.2$; $\tau_r = 0.2$, 0.3, and 0.4; and $\tau_a = \tau_r/4$. These parameters were estimated using the observed data for various insects [1–4]. For the case shown in Fig. 2b, the waveform of the feathering motion is symmetrical with respect to the reversal

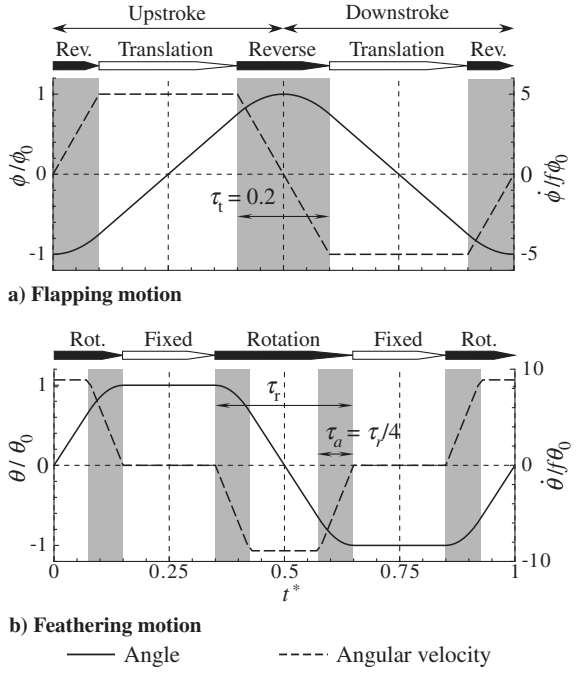

Fig. 2 Time histories of angle and angular velocity of wing kinematics in the trapez–trapez type (when $\tau_r = 0.3$ and $\tau_f = 0$).

points ($t^* = 0$ and 0.5) and is referred to as symmetrical rotation. If the rotational phase starts earlier or later than symmetrical rotation, then this motion is called advanced rotation or delayed rotation, respectively [7]. The timing of rotation is denoted by nondimensional time shift τ_f from the symmetrical rotation. Advanced rotation is denoted by $\tau_f < 0$, and delayed rotation is denoted by $\tau_f > 0$.

In sinusoidal-type flapping and feathering motions, the time histories of the angular velocities are represented as sinusoidal functions. Therefore, the time histories of the flapping and feathering angles are also represented as sinusoidal functions. In our experiments, however, we used an approximate sinusoidal motion instead of actual sinusoidal motion because of the limitations of the driving motor controller we used. The time history of the angular velocity in approximate sinusoidal motion is represented as a trapezoidal function to substitute for an actual sinusoidal function. The waveform of the approximate sinusoidal type was fitted with that of the true sinusoidal type using nonlinear least squares. From the calculation, it can be seen that when the duration of acceleration (τ_t in flapping and $2\tau_a$ in feathering) is 0.333, the waveform for the angle of the approximate sinusoidal type most closely matches that of the true sinusoidal type. The time histories of the well-matched approximate sinusoidal type are shown in Fig. 3. The true sinusoidal type is characterized by a wing accelerating or decelerating continuously during the flapping motion and rotating consistently during the feathering motion. The approximate sinusoidal flapping motion is characterized by a longer duration of flapping stroke reversal than the trapezoidal flapping motion, although it has flapping translational phases unlike the true sinusoidal type. The approximate sinusoidal feathering motion is considered to be a trapezoidal feathering motion with the duration of rotation τ_r of 0.5, because it consists entirely of rotational phases without a fixed-angle phase. The time history of fluid forces and time-averaged values between the approximate and true sinusoidal types are compared using numerical simulations in the Appendix. As shown in Figs. A1 and A2, the time-varying forces are in good agreement between the two cases in hovering and forward flight. Unless noted otherwise, the well-matched approximate sinusoidal type is called a sinusoidal type in this paper.

We used three combinations of flapping and feathering motion types: sinusoidal types for both flapping and feathering (sine–sine type), sinusoidal flapping and trapezoidal feathering (sine–trapez type), and trapezoidal types for both flapping and feathering (trapez–trapez type).

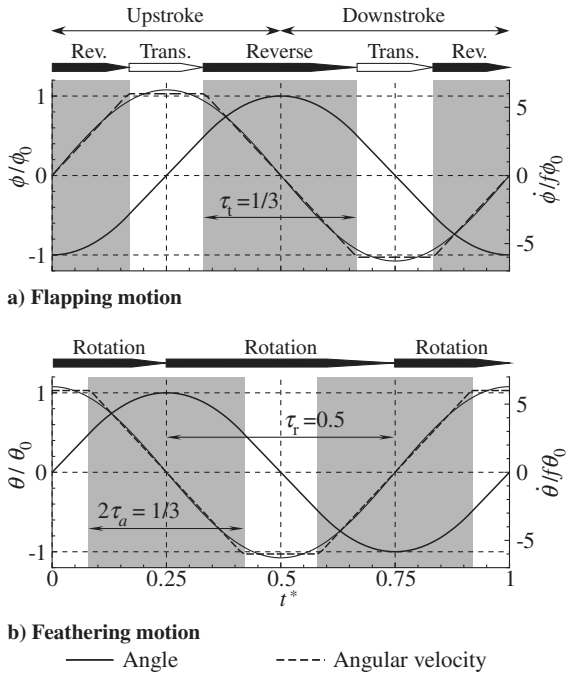

Fig. 3 Time histories of angle and angular velocity of wing kinematics in the sine–sine type (when $\tau_f = 0$).

B. Dynamically Scaled Mechanical Model for Force Measurement

We used a dynamically scaled mechanical model of a flapping wing to measure unsteady aerodynamic forces. The scaled mechanical apparatus is illustrated in Fig. 4. The flapping and feathering motions were driven by two stepping motors. The two motions were controlled independently using a controller. The motor for the flapping motion was connected to the flapping axis through gears. The motor for the feathering motion was placed on a box fixed to the flapping axis; therefore, the motor rotated with the flapping motion. A rectangular beam passed through the box and connected the motor for the feathering motion to the wing base. Since a single wing was attached to this apparatus, the wing–wing interaction, such as clap and fling, is not considered in this study.

The rectangular beam was used as a one-dimensional force/torque transducer and mounted with two sets of strain gauges wired to form a two-active gauge method; this was to measure bending moments at two different locations of the beam. Although it was difficult to measure the distribution of fluid force on the wing, we could calculate the total force acting on the wing from the difference between bending moments at the two locations [19].

The force/torque transducer had nonlinearity of less than 0.07%. The signals from the force/torque transducer were processed through a signal conditioner/amplifier and filtered using a low-pass filter with a cutoff frequency of 10 Hz. The filtered signals were input into a data acquisition device. In addition, a timing signal from the motor controller was simultaneously input into the data acquisition device in order to relate the force data to the wing kinematics. The measured force data were averaged during eight flapping cycles (7th–14th) in hovering flight and seven flapping cycles (3rd–9th) in forward flight. Figure 5 shows an example of the time history of normal fluid force coefficient and time-averaged lift and thrust coefficients for each cycle in hovering flight. Similar aerodynamic force waveforms appear after the first few cycles. The generated fluid force is symmetrical between the upstroke and downstroke in hovering flight; as a result, the thrust coefficient is canceled out and almost zero.

A normal force to the wing surface and a torque around the flapping axis were measured. The fluid force tangential to a thin flat wing is known to be very small compared with the normal fluid force [7,10]. Since the aerodynamic torque around the feathering axis is generally very small compared with the aerodynamic torque around the flapping axis [14], the aerodynamic torque around the feathering axis was not measured. The aerodynamic torque around the flapping axis M_t was interpolated using the measured bending moments at the two locations of the beam. The aerodynamic power P required for the flapping motion is given by

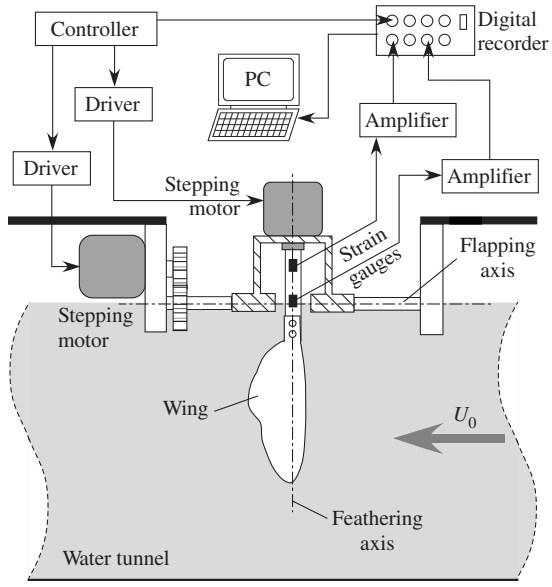

Fig. 4 Dynamically scaled mechanical model for force measurement.

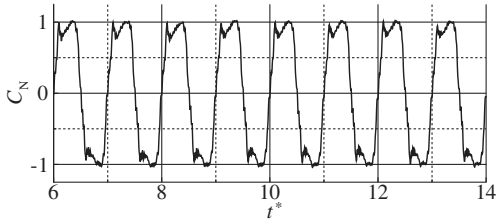

a) Time history of C_N from 7th to 14th cycles

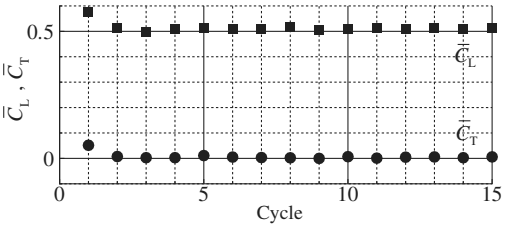

b) Time-averaged force coefficients for each cycle

Fig. 5 Similarity of generated fluid forces for flapping cycles (when trapez–trapez type, $\tau_r = 0.2$, $\tau_f = 0$, and $J = 0$).

$$P = M_t\dot{\phi} \tag{1}$$

Note that the measured forces and torques include the gravitational, buoyant, and inertial contributions in addition to the aerodynamic force and torque. Therefore, we must subtract these unnecessary forces and torques from the measured data. The gravitational and buoyant forces were measured in water at a very slow flapping frequency of 0.01 Hz. Since the contribution of inertia is very small, it was estimated from the measured data in air at faster flapping frequencies. Figure 6 shows an example of the time histories of the fluid, gravitational, and inertial forces at the flapping frequency of 0.35 Hz.

The flapping apparatus was placed over a circuit water tunnel. The size of the water tunnel was 6 m long × 3 m wide, and it had a test section with dimensions of 1.9 mlong × 0.75 m wide × 0.38 m high. The water velocity ranged from 0.02 to 0.2 m/s; the nonuniformity of velocity was less than 2% across the test section of the water tunnel. When the water surface reached the flapping axis, the height of the water was 0.36 m.

The test wing was a thin flat plate with a span length of 100 mm and a thickness of 1 mm. The edge around the wing was a square shape. To minimize the gravitational and inertial contributions, the test wing was made of an acrylic plate embedded inside an aluminum frame (Young's modulus: 72.4 GPa). The planform of the test wing was similar to that of a bumblebee, which has two forewings and two hindwings. The hindwings do not move independently and are coupled with the forewings. In this study, we considered both the forewings and hindwings as a single wing, as shown in Fig. 7. The test wing was considered to be a rigid wing, because its deformation was very small. In our experiments, the maximum deformation of the wing tip was not more than 1 mm. The wing area S is 3055 mm^2, the moment of inertia around the flapping axis I_{zw} is 1.685×10^{-5} m^4,

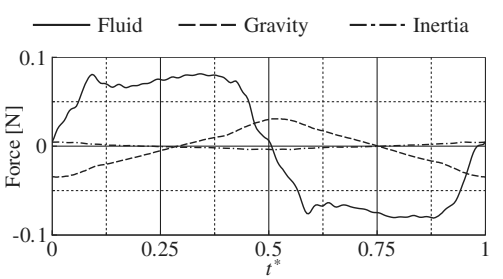

Fig. 6 Time histories of fluid, gravitational, and inertial forces (when trapez–trapez type, $\tau_r = 0.2$, $\tau_f = 0$, $f = 0.35$ Hz, and $J = 0$).

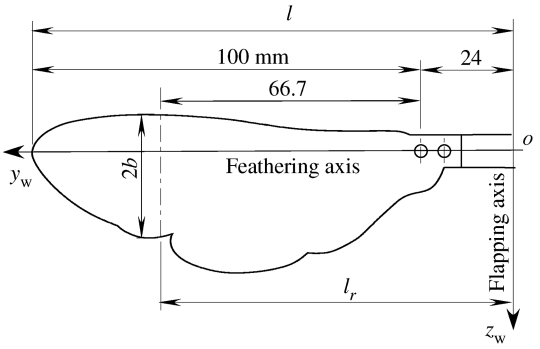

Fig. 7 Planform of test wing.

and the feathering axis is placed at the 29.5% chord length from the leading edge at the 2/3 semispan location ($y_w = l_r$).

Three nondimensional parameters are required for accurate dynamic scaling of the forces and flows obtained via the scaled model: Reynolds number, reduced frequency, and advance ratio. The reference length b was 15.75 mm; this is defined as the semichord length at 2/3 the semispan location, where the bumblebee has the maximum chord length of its forewing. The reference velocity V_0 was defined on the basis of the maximum flapping velocity for the sinusoidal flapping motion and is given by

$$V_0 = 2\pi f \phi_0 l_r \tag{2}$$

where l_r is the length from the flapping axis to the reference chord, f is the flapping frequency, and ϕ_0 is the amplitude of flapping angle. In our experiment, the wing base was placed at a distance of 24 mm from the flapping axis; therefore, $l_r = 90.7$ mm.

The Reynolds number, reduced frequency, and advance ratio are defined as follows:

$$Re = V_0 b/\nu, \qquad k = 2\pi f b/V_0, \qquad J = U_0/V_0 \tag{3}$$

where ν is the kinematic viscosity and U_0 is the forward velocity. Although the literature [2] shows that the bumblebee changes the amplitudes of the flapping and feathering angles with respect to the advance ratio, the amplitudes of the flapping and feathering motions were fixed at 60 and 45 deg, respectively, in all the experiments; then, $k = 0.166$. The Reynolds number of the bumblebee is 1980, which was calculated from Eq. (3) based on the measured data in [2]. Our measurement was conducted in the range of $Re = 1800$–4700; the flapping frequency in relation to the Reynolds number range was 0.2–0.5 Hz. The data measured at different flapping frequencies in the range were averaged because the noise dependent on the flapping frequency, such as the effect of water surface wave, was canceled. Figure 8 shows an example of the Reynolds number effect on the lift coefficients in hovering flight plotted by each timing of rotation. As shown in Fig. 8, the Reynolds number had a small effect on the aerodynamic characteristics of the flapping wing in this range.

The measured fluid forces and aerodynamic power are nondimensionalized as follows:

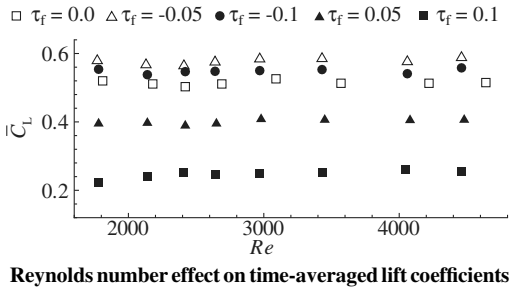

Fig. 8 Reynolds number effect on time-averaged lift coefficients plotted by each timing of rotation (when trapez–trapez type, $\tau_r = 0.2$, and $J = 0$).

$$C_N = F_n/(0.5\rho V_0^2 S), \qquad C_L = L/(0.5\rho V_0^2 S)$$
$$C_T = T/(0.5\rho V_0^2 S) \tag{4}$$

$$C_P = P/(0.5\rho V_0^3 S) \tag{5}$$

where S is the wing area and ρ is the density of fluid. Propulsive efficiency is generally defined as

$$\eta = \bar{T}U_0/\bar{P} \tag{6}$$

In hovering or horizontal forward flight, lift does no work on the body of the insect, since the body does not move in the vertical direction. We considered the ratio of $\bar{C}_L/\bar{C}_P$ as the efficiency of lift in this study.

III. Results and Discussion in Hovering Flight

A. Comparison of Time-Averaged Aerodynamic Characteristics Among Motion Types

In this section, we compare the time-averaged aerodynamic characteristics for symmetrical rotation in hovering flight among the three combinations of flapping and feathering motion types: sine–sine, sine–trapez, and trapez–trapez. Figure 9 shows the relation of $\bar{C}_L$, $\bar{C}_P$, and $\bar{C}_L/\bar{C}_P$ to the duration of rotation plotted by each combination of motion type. The sinusoidal feathering motion can be considered as $\tau_r = 0.5$, as explained previously.

First, we compare the time-averaged aerodynamic characteristics in the two types of flapping motion. $\bar{C}_L$ and $\bar{C}_P$ for the sinusoidal flapping motion are larger than those for the trapezoidal one; however, $\bar{C}_L/\bar{C}_P$ for the sinusoidal flapping motion is smaller than that for the trapezoidal one. These results indicate that the sinusoidal flapping motion generates larger lift but requires much more aerodynamic power; as a result, it has lower efficiency than the trapezoidal flapping motion.

Next, we compare the time-averaged aerodynamic characteristics in the two types of feathering motion. With a shorter duration of rotation, $\bar{C}_L$ increases and $\bar{C}_P$ decreases; therefore, $\bar{C}_L/\bar{C}_P$ increases. The sinusoidal feathering motion (sine–sine type), which has the slowest rotational motion, generates smaller lift and needs more aerodynamic power; therefore, it has lower efficiency than the trapezoidal feathering motion (sine–trapez type). These results indicate that the trapezoidal feathering motion with a shorter duration of rotation generates larger lift and requires less aerodynamic power; as a result, it has higher efficiency than the sinusoidal feathering motion.

From the observed data of the insects wing kinematics [2,4], many insects employ the trapez–trapez type. From our experimental results, the insects probably attach importance to a good efficiency in selecting the wing kinematics. In the following sections, we discuss the time histories of aerodynamic forces and explain the reason for the relations of the time-averaged aerodynamic characteristics among the motion types.

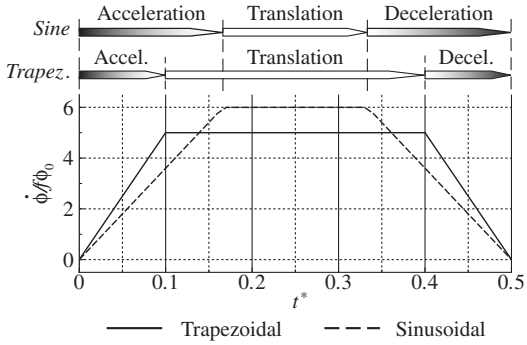

Fig. 10 Comparison of flapping angular velocity between sinusoidal and trapezoidal types.

B. Discussion on Effect of Flapping Motion Types

The difference in the time-averaged aerodynamic characteristics between the sinusoidal and trapezoidal types of flapping motion can be mainly explained as the difference in time histories of the flapping velocity. If the amplitude of the flapping angle and flapping frequency are the same between the sinusoidal and trapezoidal types of flapping motion, the time-averaged flapping velocities are the same in the two types. However, the maximum flapping velocity of the sinusoidal type is larger than that of the trapezoidal type because of the moderate acceleration and deceleration of the sinusoidal type, as shown in Fig. 10. The sinusoidal flapping motion has a 9% larger mean-squared flapping velocity and a 23% larger mean-cubed flapping velocity than the trapezoidal one. Lift and aerodynamic power are clearly proportional to the squared and cubed velocity, respectively. Therefore, the sinusoidal flapping motion generates more lift but requires much more aerodynamic power than the trapezoidal flapping motion. This explanation agrees with $\bar{C}_L$ and $\bar{C}_P$, shown in Fig. 9. For example, the sine–trapez type with $\tau_r = 0.2$ has 12% larger $\bar{C}_L$ and 24% larger $\bar{C}_P$ than the trapez–trapez type with $\tau_r = 0.2$, where the two cases have different flapping motions with the same feathering motion. These increments of $\bar{C}_L$ and $\bar{C}_P$ agree well with those of the mean-squared and mean-cubed velocities, respectively.

We explained the effect of the flapping motion type based on quasi-steady aerodynamics but did not consider unsteady aerodynamics. The aerodynamic effect due to the flapping motion obviously includes some unsteady effects such as delayed stall, wake capture, and added mass effects. The delayed stall effect, which is the main aerodynamic effect of flapping motion, is considered to be a steady effect if the wing is rotating around a flapping axis at a constant flapping velocity and constant angle of attack (i.e., combination

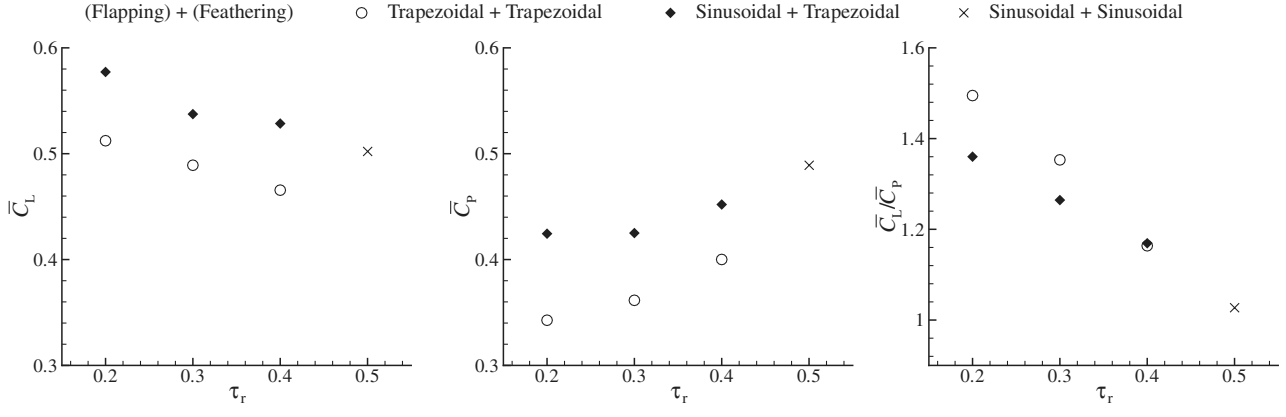

a) Lift coefficient **b) Power coefficient** **c) Efficiency of lift**

Fig. 9 Comparison of time-averaged aerodynamic characteristics for motion types in hovering flight (when $\tau_f = 0$).

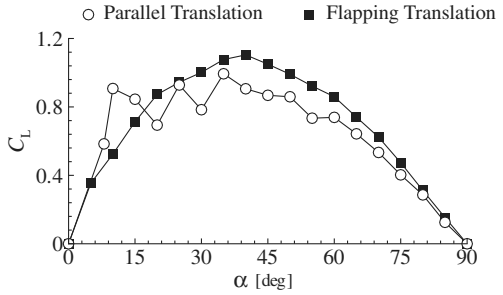

Fig. 11 Relation of lift coefficient to angle of attack between parallel and flapping translations.

of the flapping translation with the fixed-angle feathering phase). In this case, the generated fluid force is stable because a conical-shaped leading-edge vortex is attached stably to the wing upper surface and never shed from the wing [28,29]. Therefore, the lift due to the delayed stall is determined by the instantaneous flapping velocity and instantaneous angle of attack. Figure 11 shows the relation of C_L to the angle of attack α between flapping and parallel translations using the test wing. The parallel translation means that the wing is not rotating around the flapping axis but translated horizontally; thus, it seems to be a fixed wing. As shown in Fig. 11, although the fixed wing experiences a stall around $\alpha = 10$ deg and unstable lift at higher α, the flapping wing generates stable larger lift than the fixed wing at higher α due to the delayed stall effect.

The contribution of the delayed stall effect to time-varying lift is quasi-steadily estimated from the instantaneous flapping velocity and angle of attack using the relation of C_L to α, shown in Fig. 11. The time histories of C_L for the quasi-steady estimation in addition to the experimental results are shown in Fig. 12 for the two cases: trapez–trapez type (Fig. 12a) and sine–trapez type (Fig. 12b), which are different flapping types with the same feathering motion for symmetrical rotation. In both cases, the waveforms of the estimation agree well with those of the experiments during the flapping

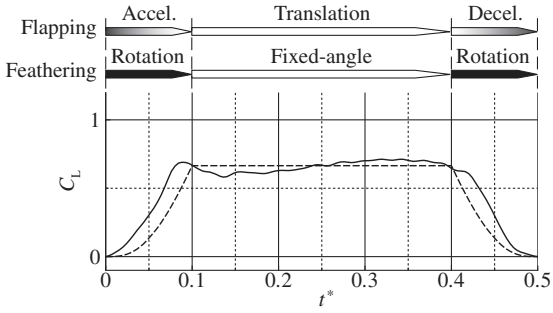

a) Trapezoidal of flapping + trapezoidal of feathering ($\tau_r = 0.2$)

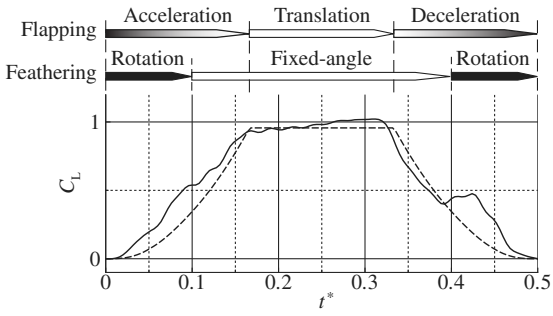

b) Sinusoidal of flapping + trapezoidal of feathering ($\tau_r = 0.2$)

Fig. 12 Quasi-steady estimation for time-varying C_L (when $\tau_f = 0$ at $J = 0$).

translation. The time-averaged lift for the quasi-steady estimation is approximately 93% of that for the experimental results, which means the delayed stall contributes approximately 93% of total lift.

There are large discrepancies in the flapping reversal phases between the estimations and experimental results, as shown in Fig. 12. These discrepancies can be attributed to the unsteady effects caused by both flapping and feathering motions: i.e., the rotational effect, wake capture, and added mass effect. These effects are strongly related to a combination of the flapping and feathering phases.

C. Discussion on Effect of Feathering Motion Types

The feathering rotational effect is the second contribution to aerodynamic force for the flapping wing. The rotational effect is obviously caused by the feathering rotation and is also related to the flapping phases, i.e., the combination of the feathering rotation with the flapping translation or reversal phase.

First, to investigate the effect of the feathering rotational speed, we discuss the two cases for advanced rotation with different durations of rotation, in which the rotational effect is emphasized. Figure 13 shows the time histories of force coefficients for advanced rotation ($\tau_f = -0.1$) with the same flapping motion but different durations of rotation: $\tau_r = 0.2$ and 0.4. In the range of $0.1 < t^* < 0.2$, both cases are in the fixed-angle phase with the flapping translation; therefore, they have good agreement in C_N, as shown in Fig. 13a. In this phase combination, the delayed stall effect is the main contribution to the aerodynamic force. Once the feathering rotation begins, C_N increases rapidly and has a peak in each case. The peak of C_N for $\tau_r = 0.2$ is 18% larger than that for $\tau_r = 0.4$. These results indicate that the pitching-up feathering rotation during the flapping translation enhances the normal fluid force; the normal fluid force increases with a shorter duration of rotation, i.e., a faster rotation. This is because the pitching-up feathering rotation enhances the vortices and circulation around the wing [13]. The enhancement of the normal fluid force due to the rotational effect results in an increase of lift, as shown in Fig. 13b; at the same time, it also increases aerodynamic power, as shown in Fig. 13c. The increase in C_P due to the rotational effect is larger than the increase in C_L. This is because the normal fluid force vector enhanced by the rotational effect is directed along the stroke plane direction because of the pitching-up feathering rotation of the wing, as shown in Fig. 13e. This means an increase in drag rather than lift. As a result, the pitching-up feathering rotation with the flapping translation causes a decrease in the efficiency of lift.

Second, to focus on the effects of the pitching-up and -down rotations with the flapping translation, we discuss the time histories of the aerodynamic forces for the two timings of rotation: $\tau_f = -0.2$ (advanced rotation) and 0.2 (delayed rotation). Figure 14 shows the time histories for the two cases in addition to the symmetrical rotation when the trapez–trapez type in $\tau_r = 0.2$. The feathering rotations in both cases are made during the flapping translation but have different rotational directions: a pitching-up rotation in the advanced rotation and a pitching-down rotation in the delayed rotation. In the pitching-up rotation, C_F and C_P for the advanced rotation are enhanced during three quarters of the feathering rotation ($0.2 < t^* < 0.35$). However, C_L is enhanced during only the first quarter of the feathering rotation ($0.2 < t^* < 0.25$); it then decreases and becomes negative during the other range ($0.25 < t^* < 0.4$). This is attributed to the inappropriate wing attitude; i.e., the fluid force vector is directed not to the upward but to the horizontal or downward direction (see Fig. 14d). On the other hand, C_F and C_P for the delayed rotation vary little during the entire pitching-down rotation ($0.1 < t^* < 0.3$). This result means that the rotational effect is not effective for the aerodynamic force during the pitching-down rotation. However, C_L for the delayed rotation is negative during the first half of the pitching-down rotation ($0.1 < t^* < 0.2$) and is smaller during the last half of the rotation ($0.2 < t^* < 0.3$) than C_L for the symmetrical rotation in the fixed-angle phase. This is attributed to the inappropriate wing attitude during the pitching-down rotation (see Fig. 14e). These discussions are summarized as follows. The pitching-up rotation during the flapping translation generates more lift but requires much more

aerodynamic power than the fixed-angle phase during the flapping translation; therefore, the efficiency decreases. The pitching-down rotation during the flapping translation is slightly effective for normal fluid force and aerodynamic power but negatively effective for lift; therefore, the efficiency decreases.

Third, in order to investigate the effect of the feathering rotation during the flapping reversal phase, we discuss the time histories of C_L and C_P for the two cases of symmetrical rotation shown in Fig. 15. The two cases are with the trapez–trapez type but the different durations of rotation; $\tau_r = 0.2$ and 0.4. The feathering rotation in $\tau_r = 0.4$ overlaps with the flapping translation in the ranges of $0.1 < t^* < 0.2$ and $0.3 < t^* < 0.4$, whereas the feathering rotation in $\tau_r = 0.2$ completely coincides with the flapping reversal phase. For the case in $\tau_r = 0.4$, the feathering rotation during the flapping translation ($0.1 < t^* < 0.2$ and $0.3 < t^* < 0.4$) causes a decrease in efficiency for the reason previously described. Although C_L increases due to the pitching-up rotation during the flapping translation when $0.3 < t^* < 0.4$, it decreases due to the pitching-down rotation when $0.1 < t^* < 0.2$, so they are canceling each other out. First, we focus on the pitching-up rotation with the flapping

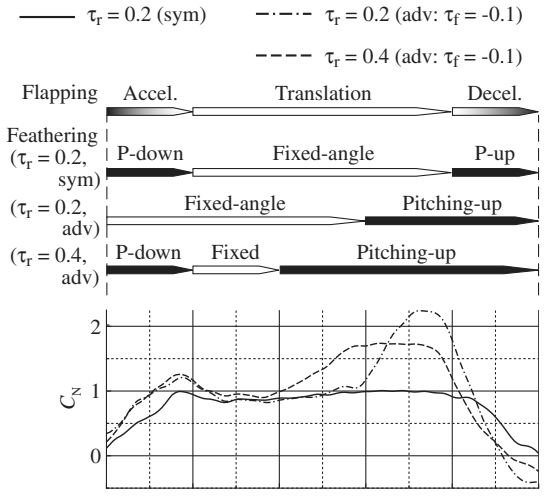

a) Normal fluid force coefficient

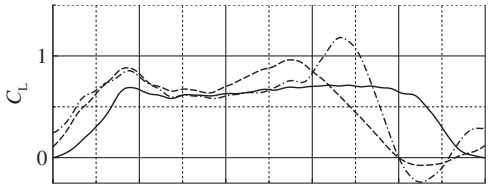

b) Lift coefficient

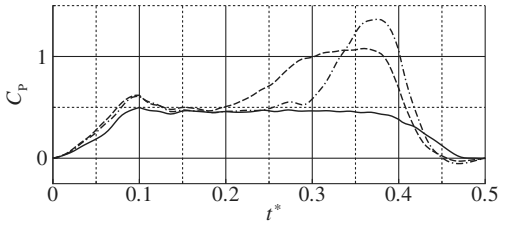

c) Power coefficient

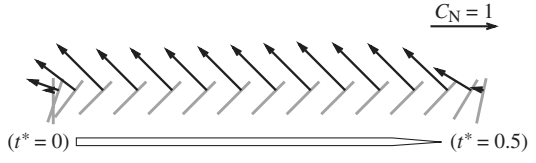

d) Fluid force vector sequence for $\tau_r = 0.2$ (sym: $\tau_f = 0.0$)

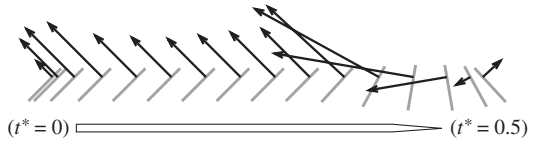

e) Fluid force vector sequence for $\tau_r = 0.2$ (adv: $\tau_f = -0.1$)

Fig. 13 Time histories of C_L and C_P for advanced rotation with different durations of rotation (when trapez–trapez type, $\tau_f = -0.1$, and $J = 0$). (sym denotes symmetrical; adv. denotes advanced.)

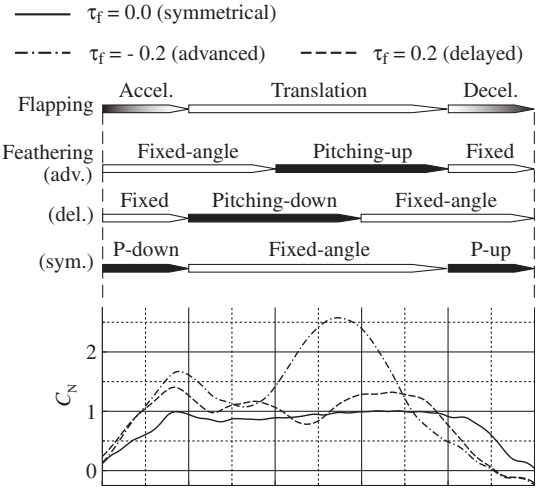

a) Normal fluid force coefficient

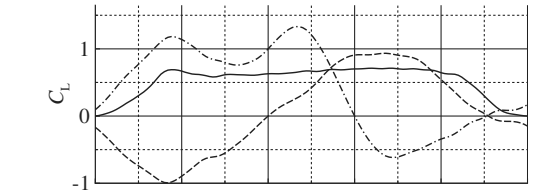

b) Lift coefficient

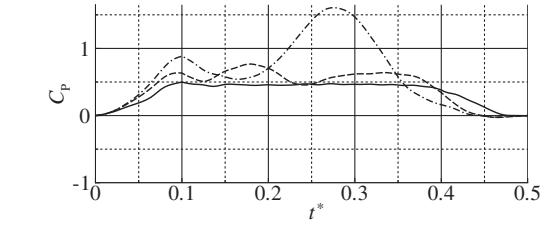

c) Power coefficient

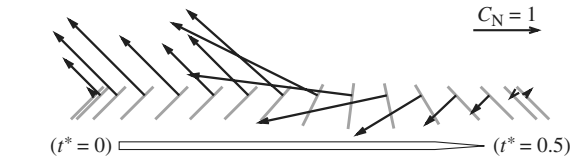

d) Fluid force vector sequence for $\tau_f = -0.2$ (advanced)

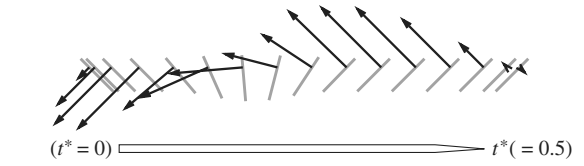

e) Fluid force vector sequence for $\tau_f = 0.2$ (delayed)

Fig. 14 Time histories of C_L and C_P in pitching-up and -down rotations (when trapez–trapez type, $\tau_r = 0.2$, and $J = 0$).

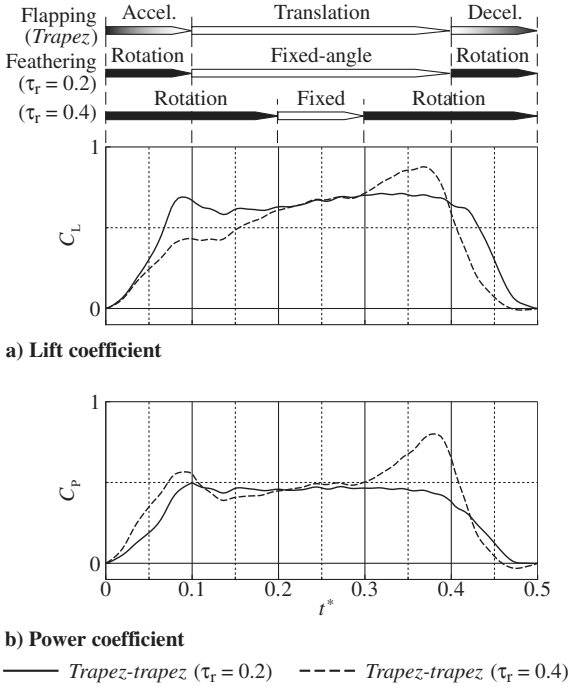

Fig. 15 Time histories of C_L and C_P for symmetrical rotation with different durations of rotation (when trapez–trapez type, $\tau_f = 0$, and $J = 0$).

deceleration ($0.4 < t^* < 0.5$). In this range, C_L in $\tau_r = 0.2$ is larger than that in $\tau_r = 0.4$ because of the faster rotation, although C_P in $\tau_r = 0.2$ is also larger. However, the increase in C_L is larger than the increase in C_P for the case in $\tau_r = 0.2$, which results in an increase in efficiency. As shown in Fig. 14, the peak for C_L ($t^* = 0.23$) in the pitching-up rotation appears before the peak for C_P ($t^* = 0.27$). Therefore, the feathering rotation with the flapping deceleration benefits from the increase in C_L but does not suffer damage to the increase in C_P. Next, we focus on the pitching-down rotation with the flapping acceleration ($0.0 < t^* < 0.1$). In this range, C_L in $\tau_r = 0.2$ is larger than that in $\tau_r = 0.4$, whereas C_P in $\tau_r = 0.2$ is smaller than that in $\tau_r = 0.4$; as a result, the efficiency of $\tau_r = 0.2$ increases. This is because the pitching-down rotation in $\tau_r = 0.2$ causes the wing to be at an appropriate attitude earlier than that in $\tau_r = 0.4$, i.e., a smaller angle of attack at a higher flapping velocity. For the case in $\tau_r = 0.4$, the wing has a higher angle of attack at a higher flapping velocity ($0.1 < t^* < 0.2$), because the rotation is not yet finished. In general, a flapping wing experiences an inappropriate attitude during and around a pitching-down rotation. Therefore, it is preferable to conduct the pitching-down rotation in a short duration and during a slower flapping velocity that is the flapping reversal phase.

Finally, we discuss the effect of the timing of rotation on the time-averaged aerodynamic characteristics. Figure 16 shows the relation of the time-averaged aerodynamic characteristics to the timing of rotation for the trapez–trapez type in the three durations of rotation. The tendencies of the time-averaged aerodynamic characteristics with respect to the timing of rotation are almost the same among the three durations of rotation. The advanced rotation, which usually includes a pitching-up rotation during the flapping translation, obtains a larger lift than any other timing of rotation but needs much more aerodynamic power; as a result, the efficiency is worse. The delayed rotation, which usually includes a pitching-down rotation during the flapping translation, causes a decrease in lift but does not affect aerodynamic power: as a result, the efficiency is worse. The symmetrical rotation, in which almost all of the rotation is made during the flapping reversal phase, shows better lift and the best efficiency. This is mainly attributable to the appropriate wing attitude for the symmetrical rotation; i.e., the flapping velocity is zero when the feathering angle is zero. From the observed data for insect wing kinematics [1,2,4], insects employ the symmetrical rotation in steady flight condition. This fact indicates that the insects attach importance to a good efficiency for the timing of rotation in steady hovering flight.

In summary, in order to benefit from the rotational effect, the pitching-up rotation should be made only during the flapping deceleration phase in terms of efficiency. When the pitching-up rotation is made during the other flapping phase, the efficiency is reduced. On the other hand, the pitching-down rotation reduces lift and efficiency because of the inappropriate wing attitude, even though it barely affects aerodynamic power. Therefore, in order to avoid loss in the pitching-down rotation, the pitching-down rotation should be made during the flapping acceleration phase (the pitching-down rotation during the flapping deceleration phase obviously includes an inappropriate wing attitude during and around the rotational phase); from this viewpoint, the symmetrical rotation is preferred. A slower rotation reduces the efficiency because lift enhancement is small and/or the wing experiences an inappropriate attitude, i.e., a higher angle of attack at a higher flapping velocity. Therefore, the trapezoidal feathering motion with the shorter duration of rotation has higher lift and efficiency, whereas the sinusoidal feathering motion, which has the longest duration of rotation, has smaller lift and efficiency than any other trapezoidal feathering motions. Although the preceding discussion is based on the results for only the fixed amplitude of the feathering angle of 45 deg, the tendency of aerodynamic characteristics with respect to the motion types may be almost unchanged at any other amplitude of the feathering angle, even if the force values are entirely shifted up- or downward. This is because these discussion is mainly based not on the flowfield around the wing but on the wing attitude. Therefore, the

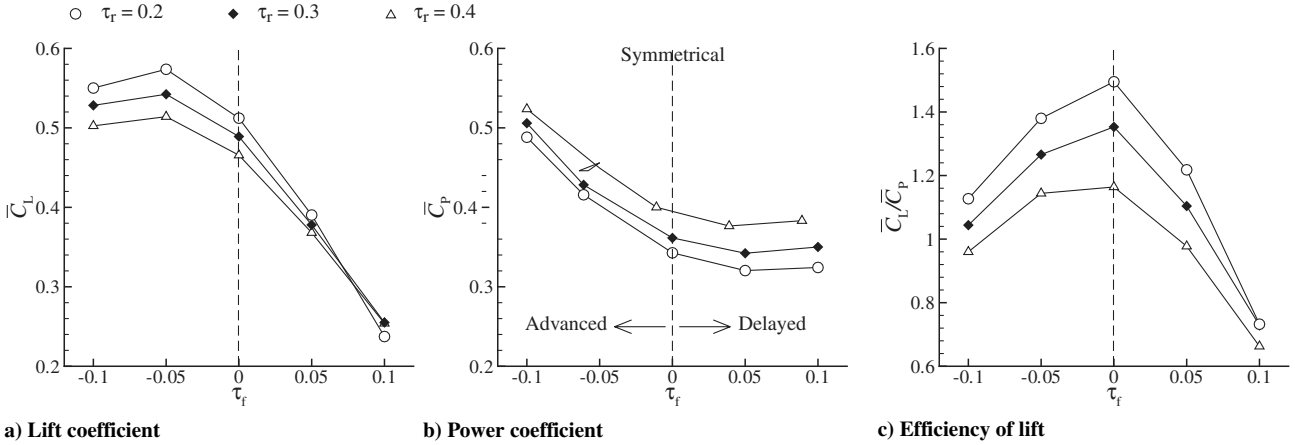

Fig. 16 Relation of time-averaged aerodynamic characteristics to timing of rotation (when trapez–trapez type at $J = 0$).

phenomena in the rotational phase may also occur at any amplitude of the feathering angle.

IV. Results and Discussion in Forward Flight

A. Comparison of Time-Averaged Aerodynamic Characteristics Among Motion Types

In this section, the time-averaged aerodynamic characteristics are compared among the motion types in forward flight. Bumblebees change the stroke plane angle with respect to the advance ratio [2]. The relations of the aerodynamic characteristics to the advance ratio and the stroke plane angle can be found in previous work by Nagai et al. [23]. The results in [23] show that the stroke plane angle of 45 deg can generate lift and thrust beyond the weight and drag of the bumblebee in all the advance ratios less than 0.5, unlike the other stroke plane angles. Therefore, we selected the fixed stroke plane angle of 45 deg as a representative angle.

Figure 17 shows the relations of the time-averaged aerodynamic characteristics with the advance ratio plotted by each combination of motion types for symmetrical rotation at $\psi = 45$ deg. In general, $\bar{C}_L$ and $\bar{C}_L/\bar{C}_P$ increase, $\bar{C}_T$ decreases with an increase in the advance ratio, and the propulsive efficiency η has a peak at an advanced ratio at any stroke plane angle [23]. Whether $\bar{C}_P$ increases or decreases with an increase in the advance ratio is dependent on the stroke plane angle; $\bar{C}_P$ decreases at $\psi = 45$ deg.

As shown in Fig. 17a, the sinusoidal flapping motion generates larger lift than the trapezoidal one at all the advance ratios. The trapezoidal feathering motion with the shorter duration of rotation generates larger lift at low advance ratios. These tendencies are the same as those in hovering flight. However, there are different tendencies at the high advance ratios; for example, $\bar{C}_L$ of the trapez–trapez type in $\tau_r = 0.4$ is larger than that in $\tau_r = 0.2$, and $\bar{C}_L$ of the sine–sine type is larger than that of the sine–trapez type in $\tau_r = 0.2$ at $J > 0.4$. These results indicate that the increasing rate of $\bar{C}_L$ with respect to the advance ratio is larger with the longer duration of rotation. As shown in Fig. 17b, the decreasing rate of $\bar{C}_T$ with respect to the advance ratio is larger with the shorter duration of rotation. For example, while $\bar{C}_T$ in $\tau_r = 0.2$ is larger than that in $\tau_r = 0.3$ at the low advance ratios, it is smaller at the high advance ratios. Every motion type generates negative thrust, or drag, at about $J > 0.5$. Therefore, the aerodynamic characteristics at $J > 0.5$ are not discussed in this study. As shown in Fig. 17c, the sine–sine type has much larger $\bar{C}_P$

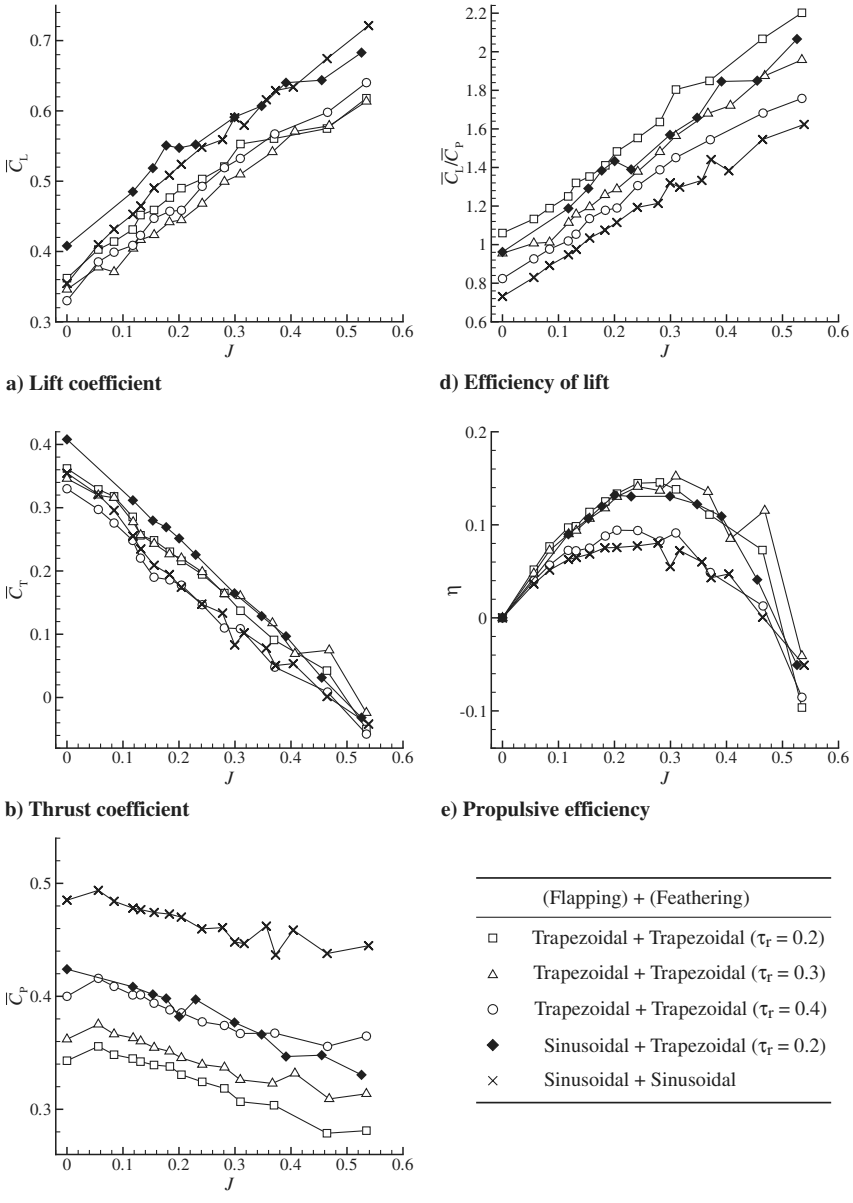

Fig. 17 Comparison of time-averaged aerodynamic characteristics among combinations of motion types in forward flight (when $\tau_f = 0$ at $\psi = 45$ deg).

than any other types for all the advance ratios. At every advance ratio, $\bar{C}_P$ decreases with shorter duration of rotation, and the trapez–trapez type in $\tau_r = 0.2$ has the smallest $\bar{C}_P$ in all the types. This tendency is the same as in hovering flight. As shown in Fig. 17d, the sine–sine type has the smallest $\bar{C}_L/\bar{C}_P$, and the trapez–trapez type in $\tau_r = 0.2$ has the largest $\bar{C}_L/\bar{C}_P$ in all the types at every advance ratio. Among the durations of rotation, $\bar{C}_L/\bar{C}_P$ increases with the shorter duration of rotation at every advance ratio. This tendency is the same as that in hovering flight. As shown in Fig. 17e, the sine–sine type has the smallest η, and the trapez–trapez types have the larger η when we only consider the range of $\eta > 0$. Although we cannot discuss the tendency at high-speed forward flight at $J > 0.5$ from our experimental results, the results at $J < 0.5$ indicate that the trapez–trapez type used by many insects provide a good efficiency for lift and thrust at slow- or intermediate-speed forward flight. In the following section, we discuss the time-varying aerodynamic forces in order to explain the tendency of the time-averaged aerodynamic characteristics.

B. Discussion of Time-Varying Aerodynamic Forces

In forward flight, a flapping wing at an inclined stroke plane angle experiences different relative inflow velocities and effective angle of attacks between the up- and downstrokes, unlike in hovering flight. The relative inflow velocity is defined by the chordwise relative flow velocity the wing experiences during the flapping motion. Figure 18 shows the time histories of the relative inflow velocity V_{in} for the trapezoidal and sinusoidal flapping motions at $J = 0.47$ and $\psi = 45$ deg. As shown in Fig. 18, the relative inflow velocity increases in the downstroke and decreases in the upstroke, unlike in hovering flight. The reason why the inflow velocity is not constant during the flapping translation is that the angle between the wing chord and the forward direction changes during the flapping translation, in which the wing rotates around the flapping axis at a constant angular velocity. For obtaining larger lift and thrust in forward flight, it is important to not only generate a larger normal force but also consider the instantaneous attitude of the wing. Figure 19 shows the time histories for the contribution ratios of normal force to lift and thrust at $\psi = 45$ deg; these were calculated from the instantaneous flapping and feathering angles and the stroke plane angle. Because of the inclined stroke plane, lift is mainly generated in the downstroke, and thrust is in the upstroke. While the sinusoidal feathering motion cannot generate lift in the upstroke and thrust in the downstroke, the trapezoidal feathering motion in

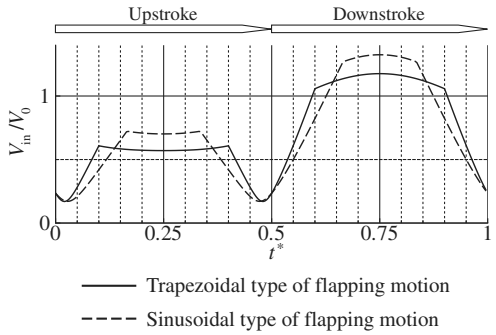

Fig. 18 Time histories of relative inflow velocity for two types of flapping motion (when $J = 0.47$ at $\psi = 45$ deg).

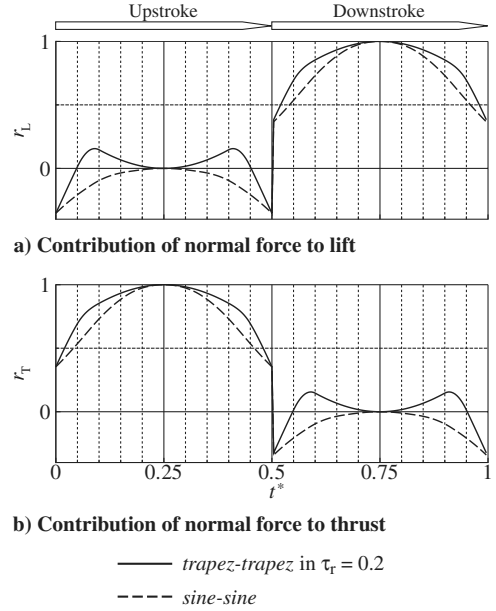

Fig. 19 Time histories of contribution ratio of normal force to lift and thrust between two motion types (when $\tau_f = 0$ at $\psi = 45$ deg).

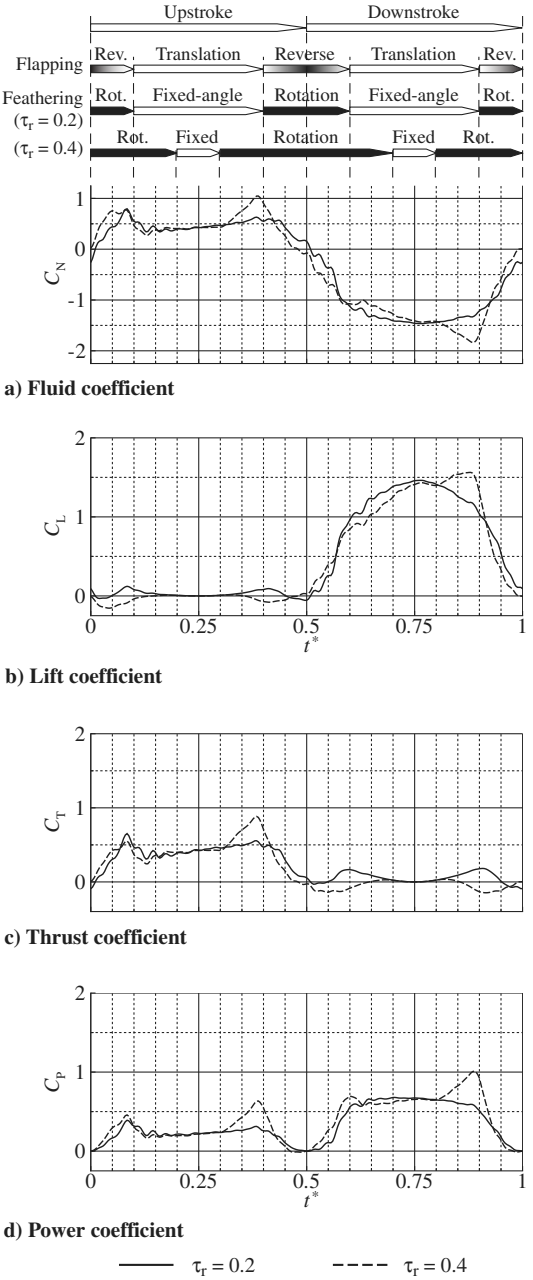

Fig. 20 Time histories of aerodynamic forces and power coefficients at $J = 0.20$ (when trapez–trapez type, $\tau_f = 0$, and $\psi = 45$ deg).

$\tau_r = 0.2$ can. This is because the trapezoidal feathering motion with the shorter duration of rotation causes the wing to be at the appropriate attitude earlier. This is one of the reasons why the trapezoidal feathering motion with the shorter duration of rotation generates larger lift and thrust in forward flight.

Figures 20 and 21 show the time histories of aerodynamic forces at $J = 0.20$ and 0.47, respectively, for the trapez–trapez types when $\tau_r = 0.2$ and 0.4 at $\psi = 45$ deg. Once the pitching-up rotation in $\tau_r = 0.4$ begins, C_F increases rapidly due to the rotational effect in both the up- and downstrokes, as shown when $0.3 < t^* < 0.4$ and $0.8 < t^* < 0.9$ of Figs. 20a and 21a. At the same time, C_P increases much more, as shown in Figs. 20d and 21d. The pitching-up rotation with the translational phase requires much more aerodynamic power, even though lift and thrust also increase, which is the same result as in hovering flight.

While the time-averaged $\bar{C}_L$ in $\tau_r = 0.2$ is larger than that in $\tau_r = 0.4$ at $J = 0.20$, it is smaller than that in $\tau_r = 0.4$ at $J = 0.47$. To explain the reason why, we focus on the waveforms of C_L at $J = 0.20$, shown in Fig. 20b. C_L in $\tau_r = 0.4$ is larger than that in $\tau_r = 0.2$ when $0.8 < t^* < 0.9$ because of the pitching-up rotation in $\tau_r = 0.4$. On the other hand, C_L in $\tau_r = 0.2$ is larger than that in $\tau_r = 0.4$ when $0.9 < t^* < 1.0$ because of the faster pitching-up rotation in $\tau_r = 0.2$, when $0.1 < t^* < 0.2$ because of the pitching-down rotation in $\tau_r = 0.4$, and in the upstroke because of the appropriate wing attitude in $\tau_r = 0.2$. Since the case in $\tau_r = 0.2$ has more preferable factors than that in $\tau_r = 0.4$, the time-averaged $\bar{C}_L$ in $\tau_r = 0.2$ is larger than that in $\tau_r = 0.4$ at $J = 0.20$. Next, we focus on the waveforms of C_L at $J = 0.47$, shown in Fig. 21b. C_L in $\tau_r = 0.4$ is also larger than that in $\tau_r = 0.2$ when $0.8 < t^* < 0.9$, which is the same result as at $J = 0.20$. In the other range, the waveform in $\tau_r = 0.2$ is similar to that in $\tau_r = 0.4$. Therefore, the time-averaged $\bar{C}_L$ in $\tau_r = 0.4$ is larger than that in $\tau_r = 0.2$. The reason why the trapezoidal feathering motion with the shorter duration of rotation generates smaller $\bar{C}_L$ at the high advance ratios than that with the longer one can be explained as follows. As shown in Fig. 20b, the upstroke is only slightly effective for lift because the relative inflow and effective angle of attack decrease with an increase in the advance ratio. In the downstroke, the relative inflow velocity is enhanced with an increase in the advance ratio, especially in the middle of the downstroke. This indicates that the contribution of the flapping reversal phase to lift is reduced relatively and that the flapping translational phase becomes relatively important. Thus, the feathering rotation with the flapping reversal phase, which plays an important role in hovering and forward flight at the low advance ratios, is only slightly effective for increasing lift, although it is still effective for increasing efficiency. Therefore, the slower rotation, which usually includes the pitching-up rotation with the flapping translation, is preferable for generating larger lift at higher advance ratios.

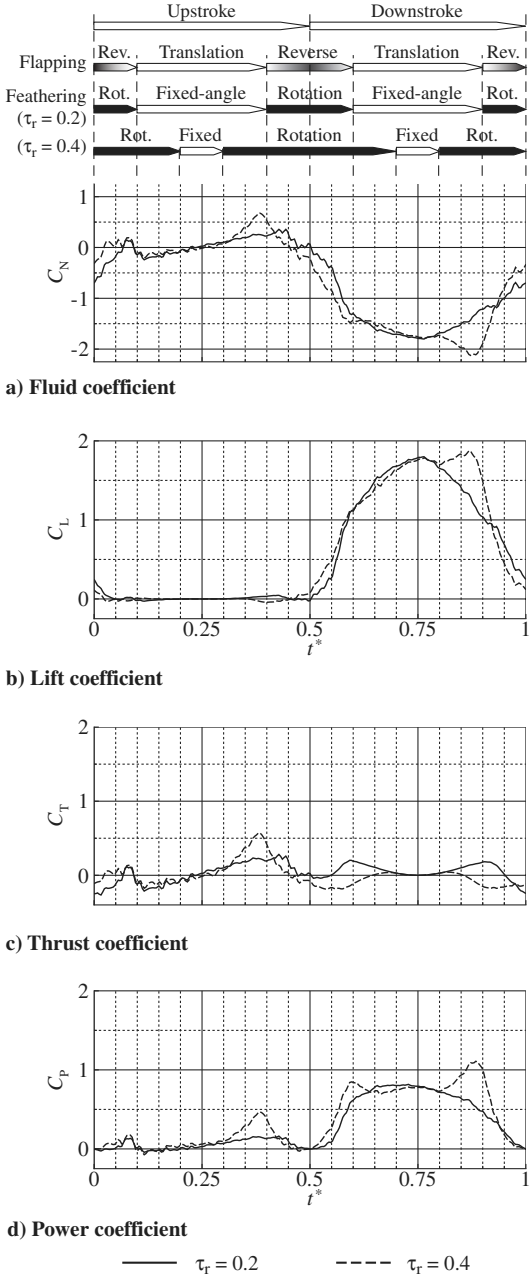

Fig. 21 Time histories of aerodynamic forces and power coefficients at $J = 0.47$ (when trapez–trapez type, $\tau_f = 0$, and $\psi = 45$ deg).

V. Conclusions

The time-varying aerodynamic forces and power of the flapping wing in hovering and forward flight has been measured using a dynamically scaled mechanical model in a water tunnel. Using the rigid wing with the planform of the bumblebee with the fixed amplitude of flapping and feathering motion at the fixed stroke plane angle, the effects of the wing kinematics on the aerodynamic characteristics have been investigated, and the aerodynamic characteristics for three combinations of motion type have been compared: trapez–trapez, sine–trapez, and sine–sine types in hovering and forward flight. The experimental results indicate that the combination of a flapping phase with a feathering phase is important for high performance in hovering and forward flight. The sinusoidal flapping motion can generate larger lift and requires much more aerodynamic power than the trapezoidal one, because the former has a larger maximum flapping velocity than the latter. The pitching-up rotation with a shorter duration of rotation enhances the normal fluid force. However, the feathering rotation during the flapping translation causes an increase in aerodynamic power rather than lift and thrust in hovering and forward flight. The feathering pitching-down rotation during the flapping translation causes a decrease in lift and efficiency because of an inappropriate wing attitude. For high efficiency, the feathering rotation should be performed during the flapping reversal phase in which the flapping velocity is slower. For these reasons, the trapezoidal flapping motion and trapezoidal feathering motion with the shorter duration of rotation should be selected in order to obtain higher efficiency in hovering and forward flight. Moreover, the symmetrical rotation should be selected for higher efficiency for the same reason. The trapez–trapez type in symmetrical rotation is employed by many insects. This fact indicates that the insects attach importance to a good efficiency in selecting the wing kinematics. The experimental results also indicate that the sinusoidal flapping motion and trapezoidal feathering motion with the shorter duration of rotation should be selected in order to obtain larger lift in hovering and intermediate speed forward flight. These results provide useful information on the design of flapping-type MAVs.

Appendix

In our experiments, the approximate sinusoidal motion was employed instead of the true sinusoidal motion because of the limitations of our driving motor controller. In this section, the aerodynamic characteristics calculated with CFD are compared between the approximate and true sinusoidal motions. The numerical simulation was conducted using the 3-D Navier–Stokes code originally developed by Isogai et al. [18], Yamamoto and Isogai [19], and Nagai et al. [23]. Details of the numerical computation can be seen in [23].

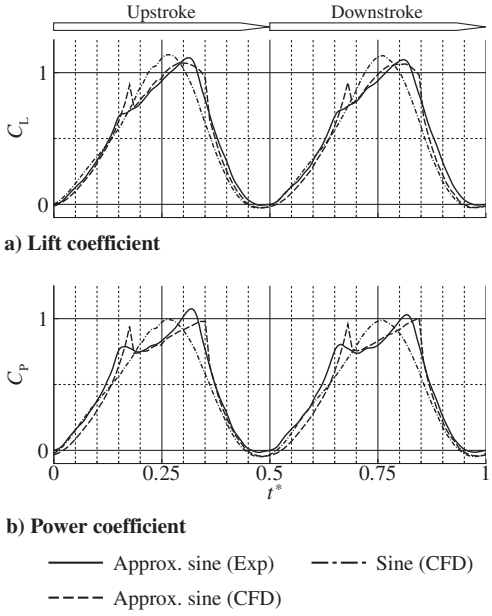

Fig. A1 Comparison of true and approximate sine–sine types calculated by numerical simulation in hovering flight (when $\tau_f = 0$ at $Re = 2409$). Sine denotes sinusoidal type.

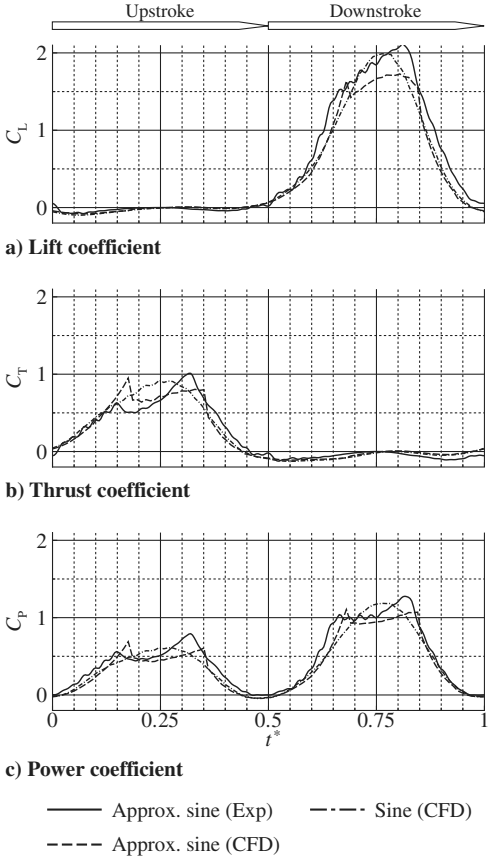

Fig. A2 Comparison of true and approximate sine–sine type calculated by numerical simulation in forward flight at $J = 0.181$ (when $\tau_f = 0$, $\psi = 45$ deg, and $Re = 3132$).

Table A1 Comparison of time-averaged aerodynamic characteristics between true and approximate sine–sine types in hovering flight[a]

	True sine (CFD)	Approx. sine (CFD)	Approx. sine (Exp)
$\bar{C}_L$	0.481	0.490	0.501
$\bar{C}_P$	0.441	0.450	0.485
$\bar{C}_L/\bar{C}_P$	1.092	1.089	1.034

[a]Sine denotes sinusoidal type.

Table A2 Comparison of time-averaged aerodynamic characteristics between true and approximate sine–sine types in forward flight at $J = 0.181$[a]

	True sine (CFD)	Approx. sine (CFD)	Approx. sine (Exp)
$\bar{C}_L$	0.435	0.411	0.508
$\bar{C}_T$	0.197	0.187	0.195
$\bar{C}_P$	0.411	0.389	0.473
$\bar{C}_L/\bar{C}_P$	1.059	1.056	1.075
η	0.868	0.870	0.753

[a]Sine denotes sinusoidal type.

Figure A1 shows the time histories of C_L and C_P in hovering flight calculated by the numerical simulation for the true and approximate sine–sine types. In addition, the experimental results for the approximate sine–sine type are shown in this figure. The waveforms of C_L and C_P are in good agreement among the true and approximate sine–sine types and the experimental result in hovering flight. The time-averaged forces and power coefficients in hovering flight are compared in Table A1 for the true and approximate sine–sine types. The time-averaged lift and power coefficients for the approximate sine–sine type are slightly larger than those for the true one, although $\bar{C}_L/\bar{C}_P$ agrees well between the two types. Figure A2 shows the time histories of C_L, C_T, and C_P in forward flight at $J = 0.181$ and $\psi = 45$ deg, calculated by the numerical simulation for the true and approximate sine–sine types in addition to the experimental result. The waveforms are in good agreement among the true and approximate sine–sine types and the experimental result in forward flight. The time-averaged coefficients in forward flight are compared in Table A2 for the true and approximate sine–sine types. $\bar{C}_L$, $\bar{C}_T$, and $\bar{C}_P$ for the true sine–sine type are larger than those for the approximate one, although $\bar{C}_L/\bar{C}_P$ and η agree well between the two types. These comparisons indicate that our experimental results are sufficiently valid to discuss the effects of flapping wing kinematics on hovering and forward flight aerodynamics.

Acknowledgments

This study was supported by the Ministry of Education, Culture, Sports, Science and Technology of Japan under the High-Tech Research Center Promotion Program. The authors would like to thank Toshiyuki Hayase of Tohoku University and Tatsumi Fujimoto of Nippon Bunri University for their support. The authors would also like to thank Takumi Ito and Keita Miura for their assistance in carrying out the experiments.

References

[1] Azuma, A., and Watanabe, T., "Flight Performance of a Dragonfly," *Journal of Experimental Biology*, Vol. 137, No. 1, 1988, pp. 221–252.

[2] Dudley, R., and Ellington, C. P., "Mechanics of Forward Flight in Bumblebees I. Kinematics and Morphology," *Journal of Experimental Biology*, Vol. 148, No. 1, 1990, pp. 19–52.

[3] Dudley, R., and Ellington, C. P., "Mechanics of Forward Flight in Bumblebees II. Quasi-Steady Lift and Power Requirements," *Journal of Experimental Biology*, Vol. 148, No. 1, 1990, pp. 53–88.

[4] Ellington, C. P., "The Aerodynamics of Hovering Insect Flight. III: Kinematics," *Philosophical Transactions of the Royal Society of London. Series B, Biological Sciences*, Vol. 305, No. 1122, 1984, pp. 41–78.
doi:10.1098/rstb.1984.0051

[5] Sane, S. P., and Dickinson, M. H., "The Control of Flight Force by a Flapping Wing: Lift and Drag Production," *Journal of Experimental Biology*, Vol. 204, No. 15, 2001, pp. 2607–2626.

[6] Sane, S. P., and Dickinson, M. H., "The Aerodynamic Effects of Wing Rotation and a Revised Quasi-Steady Model of Flapping Flight," *Journal of Experimental Biology*, Vol. 205, 2002, pp. 1087–1096.

[7] Dickinson, M. H., Lehmann, F. -O., and Sane, S. P., "Wing Rotation and the Aerodynamic Basis of Insect Flight," *Science*, Vol. 284, No. 5422, 1999, pp. 1954–1960.
doi:10.1126/science.284.5422.1954

[8] Birch, J. M., and Dickinson, M. H., "The Influence of Wing-Wake Interactions on the Production of Aerodynamic Forces in Flapping Flight," *Journal of Experimental Biology*, Vol. 206, No. 13, 2003, pp. 2257–2272.
doi:10.1242/jeb.00381

[9] Lehmann, F. -O., Sane, S. P., and Dickinson, M. H., "The Aerodynamic Effects of Wing-Wing Interaction in Flapping Insect Wings," *Journal of Experimental Biology*, Vol. 208, No. 16, 2005, pp. 3075–3092.
doi:10.1242/jeb.01744

[10] Birch, M. J., Dickson, W. B., and Dickinson, M. H., "Force Production and Flow Structure of the Leading Edge Vortex on Flapping Wings at High and Low Reynolds Numbers," *Journal of Experimental Biology*, Vol. 207, No. 7, 2004, pp. 1063–1072.
doi:10.1242/jeb.00848

[11] Dickson, W. B., and Dickinson, M. H., "The Effect of Advance Ratio on the Aerodynamics of Revolving Wing," *Journal of Experimental Biology*, Vol. 207, No. 24, 2004, pp. 4269–4281.
doi:10.1242/jeb.01266

[12] Maybury, W. J., and Lehmann, F. -O., "The Fluid Dynamic of Flight Control by Kinematic Phase Lag Variation between Two Robotic Insect Wings," *Journal of Experimental Biology*, Vol. 207, No. 26, 2004, pp. 4707–4726.
doi:10.1242/jeb.01319

[13] Sun, M., and Tang, J., "Unsteady Aerodynamic Force Generation by a Model Fruit Fly Wing in Flapping Motion," *Journal of Experimental Biology*, Vol. 205, No. 1, 2002, pp. 55–70.

[14] Sun, M., and Tang, J., "Lift and Power Requirements of Hovering Flight in *Drosophila Virilis*," *Journal of Experimental Biology*, Vol. 205, No. 16, 2002, pp. 2413–2427.

[15] Wang, J., and Sun, M., "A Computational Study of the Aerodynamics and Forewing–Hindwing Interaction of a Model Dragonfly in Forward Flight," *Journal of Experimental Biology*, Vol. 208, No. 19, 2005, pp. 3785–3804.
doi:10.1242/jeb.01852

[16] Sun, M., and Wu, J. H., "Aerodynamic Force Generation and Power Requirements in Forward Flight in a Fruit Fly with Modeled Wing Motion," *Journal of Experimental Biology*, Vol. 206, No. 17, 2003, pp. 3065–3083.
doi:10.1242/jeb.00517

[17] Sun, M., and Lan, S., "A Computational Study of the Aerodynamic Forces and Power Requirements of Dragonfly (*Aeschna Juncea*) Hovering," *Journal of Experimental Biology*, Vol. 207, No. 11, 2004, pp. 1887–1901.
doi:10.1242/jeb.00969

[18] Isogai, K., Fujishiro, S., Saitoh, T., Yamasaki, M., and Matsubara, M., "Unsteady Three-Dimensional Viscous Flow Simulation of Dragonfly Hovering," *AIAA Journal*, Vol. 42, No. 10, 2004, pp. 2053–2058.
doi:10.2514/1.6274

[19] Yamamoto, M., and Isogai, K., "Measurement of Unsteady Fluid Dynamic Forces for a Mechanical Dragonfly Model," *AIAA Journal*, Vol. 43, No. 12, 2005, pp. 2475–2480.
doi:10.2514/1.15899

[20] Liu, H., Ellington, C. P., Kawachi, K., Van Den Berg, C., and Willmott, A. P., "A Computational Fluid Dynamic Study of Hawkmoth Hovering," *Journal of Experimental Biology*, Vol. 201, 1998, pp. 461–477.

[21] Aono, H., and Liu, H., "Vortical Structure and Aerodynamics of Hawkmoth Hovering," *Journal of Biomechanical Science and Engineering*, Vol. 1, No. 1, 2006, pp. 234–245.
doi:10.1299/jbse.1.234

[22] Aono, H., Liang, F., and Liu, H., "Near- and Far-Field Aerodynamics in Insect Hovering Flight: an Integrated Computational Study," *Journal of Experimental Biology*, Vol. 211, No. 2, 2008, pp. 239–257.
doi:10.1242/jeb.008649

[23] Nagai, H., Isogai, K., Fujimoto, T., and Hayase, T., "Experimental and Numerical Study of Forward Flight Aerodynamics of Insect Flapping Wing," *AIAA Journal*, Vol. 47, No. 3, 2009, pp. 730–742.
doi:10.2514/1.39462

[24] Kaya, M., and Tuncer, I. H., "Nonsinusoidal Path Optimization of a Flapping Airfoil," *AIAA Journal*, Vol. 45, No. 8, 2007, pp. 2075–2082.
doi:10.2514/1.29478

[25] Tang, J., Viieru, D., and Shyy, W., "Effects of Reynolds Number and Flapping Kinematics on Hovering Aerodynamics," *AIAA Journal*, Vol. 46, No. 4, 2008, pp. 967–976.
doi:10.2514/1.32191

[26] Bos, F. M., Lentink, D., Van Oudheusden, B. W., and Bijl, H., "Influence of Wing Kinematics on Aerodynamic Performance in Hovering Insect Flight," *Journal of Fluid Mechanics*, Vol. 594, 2008, pp. 341–368.
doi:10.1017/S0022112007009172

[27] Wang, Z. J., Birch, J. M., and Dickinson, M. H., "Unsteady Forces and Flows in Low Reynolds Number Hovering Flight: Two-Dimensional Computation vs Robotic Wing Experiments," *Journal of Experimental Biology*, Vol. 207, No. 3, 2004, pp. 449–460.
doi:10.1242/jeb.00739

[28] Ellington, C. P., Van den Berg, C., Willmott, A. P., and Thomas, A. L. R., "Leading-Edge Vortices in Insect Flight," *Nature*, Vol. 384, No. 6610, 1996, pp. 626–630.
doi:10.1038/384626a0

[29] Usherwood, J. R., and Ellington, C. P., "The Aerodynamics of Revolving Wings I. Model Hawkmoth Wings," *Journal of Experimental Biology*, Vol. 205, No. 11, 2002, pp. 1547–1564.

P. Beran
Associate Editor